Science of the Total Environment 917 (2024) 170343

Contents lists available at ScienceDirect

Science of the Total Environment

journal homepage: www.elsevier.com/locate/scitotenv

Trapping and bypassing of suspended particulate matter, particulate nutrients and faecal indicator organisms in the river-estuary transition zone of a shallow macrotidal estuary

Colin Jago [a], Peter Robins [a,*], Eleanor Howlett [a,b], Francis Hassard [a,c,d], Paulina Rajko-Nenow [a], Suzanna Jackson [a,b], Nguyen Chien [a], Shelagh Malham [a]

[a] School of Ocean Sciences, Bangor University, Marine Centre Wales, Menai Bridge LL59 5AB, UK
[b] Natural Resources Wales, Maes y Ffynnon, Penrhos Rd, Penrhosgarnedd, Bangor LL57 2DW, UK
[c] Cranfield University, College Way, Bedford MK43 0AL, UK
[d] Institute for Nanotechnology and Water Sustainability, College of Science, Engineering and Technology, University of South Africa, Johannesburg, South Africa

HIGHLIGHTS

- Estuary ebb-dominance of turbulence was observed in the RETZ.
- The RETZ was found to be a conduit for SPM rather than a zone of accumulation.
- Complex size fractionation and biogeochemical exchanges of particulates were observed.
- SPM concentrations in the ETM exceeded microbial water quality standards.
- These results are transferable to embayment-type estuaries on macrotidal coasts.

GRAPHICAL ABSTRACT

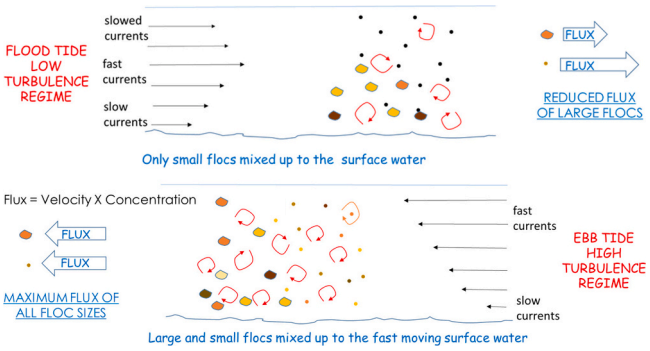

ARTICLE INFO

Editor: Jose Julio Ortega-Calvo

Keywords:
Estuary
Axial convergent front
Turbulence
Conwy

ABSTRACT

Hydrodynamic controls of the transport of suspended particulate matter (SPM), particulate nutrients and faecal indicator organisms (FIOs) in the river-estuary transition zone (RETZ) of a shallow macrotidal estuary were studied on tidal and seasonal timescales. The RETZ was found to be a conduit for SPM rather than a zone of particle accumulation during spring tides, with complex size fractionation and biogeochemical exchanges of particulate nutrient/FIO compositions. The downstream RETZ was characterised by flood-dominant currents, but with ebb-dominant turbulence due to the suppression of flood tide turbulence by salinity stratification created by lateral convergence; this produced a net seaward mass transport of SPM. Without lateral convergence in the narrower upstream RETZ, flood-dominant currents and flood-dominant turbulence were experienced. Hence the RETZ exported SPM landwards from its upper end and seawards from its lower end — a process observed throughout the year during spring tides and low-to-mean river flows. During neap tides when SPM concentrations were reduced, the RETZ became a zone of minor particle accumulation as its lower end imported SPM landwards from the estuary and its upper end imported SPM seawards from the river. During a river flood event,

* Corresponding author.
E-mail address: p.robins@bangor.ac.uk (P. Robins).

https://doi.org/10.1016/j.scitotenv.2024.170343
Received 28 September 2023; Received in revised form 19 January 2024; Accepted 19 January 2024
Available online 26 January 2024

net SPM flux was significantly increased and was seawards throughout the RETZ. SPM mass concentration and carbon, nitrogen, phosphorous, and FIO concentrations peaked due to local resuspension and advection of an ephemeral estuarine turbidity maximum (ETM). The ETM formed on the advancing flood tide due to entrainment of material from intertidal flats. Flocculation and settling occurred at high slack water. The ETM was reconstituted by entrainment on the ebb and was composed of larger flocs than on the flood. Particulate nutrients and FIOs were associated with flocs in the 10–200 μm range but not with smaller or larger flocs. SPM concentrations in the resuspension component and ETM exceeded microbial water quality standards, emphasising the need for monitoring practices that consider tidal dynamics. The results from this study showing periodic SPM export from, rather than prolonged accumulation in, the RETZ and the influence of particle size fractionation on biogeochemical fluxes in the RETZ, are likely to be transferable to many other embayment-type estuaries on macrotidal coasts.

1. Introduction

The River-Estuary Transition Zone (RETZ) is the region where fresh water from the tidally influenced river and saltwater from the upper estuary converge. This convergence gives rise to strong gradients in water dynamics and suspended material that vary markedly over tidal to seasonal time scales. The majority of biogeochemical components (e.g., nutrients) and biological components (e.g., microorganisms including pathogens) from land runoff to the river network will traverse the RETZ in order to reach the coast and sea. Consequently, the RETZ serves as a globally significant interface from land to sea (Levin et al., 2001).

Suspended particulate matter (SPM), which includes remobilised sediments and microplastics, can be key mediators of biogeochemical and biological fluxes through estuaries. This is because particles carry carbon (Smith et al., 1992) and other nutrients, along with microbial pathogens (Malham et al., 2014). Adhesion to SPM provides pathogens with favourable survival conditions, protects them from UV and salinity, and provides an energy source (Perkins et al., 2014). The association of these components with SPM is considerably enhanced by the contribution of flocculated particles whose large internal and external surface areas increase the adhesion of biogeochemical components and provide favourable conditions for pathogen survival (Hassard et al., 2016). Flocs are complex aggregates of inorganic and organic components, extracellular polymeric material, and water (Droppo, 2001) characterised by multidimensional, fragile structures, low density, and overall sizes that vary widely over several orders of magnitude. It is known that in the marine environment floc size and properties vary on a range of time scales from tidal (e.g., Jago et al., 1993; Jago and Jones, 1998) to seasonal (e.g., Jago et al., 2007), being particularly sensitive to tidally-varying turbulence. Low-intensity turbulence improves flocculation rates, while high-intensity turbulence influences floc rupture (Jago et al., 2006a). Additionally, the seasonally varying biological production of sticky polymers including carbohydrates, particularly by microplankton enhances flocculation (Jago et al., 2007). However, there remains a lack of data about floc properties and their variability in the RETZ although the strong gradients of the RETZ suggest that this variability is probably important. Floc properties determine settling, resuspension, and advection of SPM, and the associated particulate biogeochemical and biological components. Therefore, understanding the flux and fate of these components in the RETZ requires new quantitative insights into the behaviour of the flocs.

Accordingly, this study sought to investigate the hydrodynamics and properties and dynamics of SPM, specifically focusing on flocs and associated biogeochemical components (carbon, nitrogen, phosphorus, faecal indicator organisms — FIOs). The study focused on the Conwy estuary, which is representative of many embayment-type macrotidal estuaries globally, and the investigation spanned the RETZ across tidal and seasonal timescales, and included the impact of river flood events. A primary objective of the study was to ascertain whether the RETZ acts as a sink or a conduit for particles and particle-associated biogeochemical components. Previous studies of the RETZ in other systems include Painchaud and Therriault, 1989; Findlay et al., 1991; Vaqué et al., 1992; Laprise and Dodson, 1994; Winkler et al., 2003; Golebiewski et al., 2017; Torres, 2017; Jones et al., 2020; Sulaiman et al., 2021; Philips, 2022. Most previous studies are not in systems that are strongly tidally mediated like the Conwy RETZ and do not focus on SPM processes. The study system, observational fieldwok, and analyses methods are described in Section 2. The results are presented in Section 3, followed by a wider discussion and conclusions drawn in Sections 4 and 5, respectively.

2. Methods

2.1. Study site

The study site, the macrotidal Conwy estuary in North Wales, UK, extends 22 km from the tidal limit at Llanwrst to the mouth near Deganwy, where it opens into the Irish Sea (Fig. 1). In both morphology and dynamics, the estuary is representative of embayment-type estuaries on macrotidal coasts. The estuary is classified as macrotidal or hypertidal (tidal range 3–7 m), with shallow water depths (7 m in the RETZ at mean high spring tide), and a mean river discharge of 18.5 $m^3 s^{-1}$ but rising to several hundred $m^3 s^{-1}$ (maximum ~920 $m^3 s^{-1}$) within a few hours during/following precipitation events (Robins et al., 2019). Under fair weather conditions, the estuary's flow ratio (tidal volume transport/freshwater discharge) is small, about 20 (Simpson et al., 2001). During the ebb tide, the estuary is emptied of saltwater, and at low tide, is characterised by extensive sand flats, traversed by a shallow, meandering freshwater channel with patchy mudflats on the margins. This morphology is typical of many macrotidal estuaries on the UK's west coast (Davidson et al., 1991) and parts of the NW European coast. The estuary also displays pronounced tidal asymmetry, characterised by short, fast flood tides and longer, slower ebb tides, which is typical of many macrotidal estuaries. Current speeds reach 1.3 m s^{-1} during the 2.75 h flood, while ebb current speeds are 25–30 % smaller.

The hydrodynamics of the estuary have been previously studied, with a primary focus on investigating the dynamics of an axial convergent front (e.g., Nunes and Simpson, 1985; Simpson et al., 2001; Robins et al., 2012; Howlett et al., 2015;) and water quality (e.g., Bashawri et al., 2020; Robins et al., 2014, 2019, 2022). Other studies have examined the microbiology of the water and sediments in the estuary (e.g., Quilliam et al., 2011; Perkins et al., 2014).

2.2. Field measurements

Bed frames instrumented with a RDI 1200 kHz Acoustic Doppler Current Profiler (ADCP), Conductivity-Temperature-Depth (CTD) and Laser In-Situ Scattering and Transmissometry (LISST) were deployed in the centre of the channel at two sites in the RETZ (Fig. 1). Station 1 (Taly-Cafn) is located in the upper estuary, 10 km from the estuary mouth, where the channel width is ~120 m and is reached by saltwater on all tides. Station 1 was chosen as a mid-estuary location, at the downstream limit of the RETZ, which was a straight section of the channel (minimising variations due to curvature) and where there was good access to the site for deployment and retrieval. Station 2 (Dolgarrog) is further upstream, 15 km from the estuary mouth, where the channel is also

straight and the width is 30 m; saltwater reaches this location, but only during spring tides and low river flows, but the station remains within the tidally influenced river at all other times. The tidal ranges can reach up to 5 m and 3 m at Tal-y-Cafn and Dolgarrog, respectively.

At each station, the bed frames were deployed in the centre of the channel for two weeks on four separate occasions: 20 September–07 October 2013; 15 January–03 February 2014; 17 March–01 April 2014; and 14–31 July 2014. This sampling strategy intended to capture both tidal variability and seasonal variability in hydrology. The Sept./Oct. 2013 deployment experienced particularly large spring tides (8.2 m tidal range), whereas the later deployments experienced spring tidal ranges of 6.7–7.5 m. River flows from the river Conwy ranged from 0.5 to 24 m^3 s^{-1} during the Sept./Oct. 2013 deployment (the mean flow is ~18.5 m^3 s^{-1}) but were higher (20–74 m^3 s^{-1}) during the Jan./Feb. 2014 deployment with peak flows around the 95th percentile value. The Mar./Apr. deployment experienced flows of 3–20 m^3 s^{-1}, while the summer (Jul. 2014) deployment experience no rainfall and river flows <6 m^3 s^{-1} (see Fig. S1, Supplementary Material). On all occasions, there was little wind present during the sampling. The LISST and CTD were positioned 0.35–0.42 m above the bed, and the ADCP 0.78 m above the bed. The ADCP and LISST were operated in burst mode, collecting data for 150 s, and then resting for 150 s, allowing for high-frequency sampling over the deployment periods, with a vertical resolution of 0.1 m for the ADCP. Instrument fouling or collision from debris led to some data loss from Tal-y-Cafn in July and September/October and from Dalgarrog in July. The only serious loss occurred at Dalgarrog in January/February when a large tree trunk knocked the bed frame out of alignment, so no valid data were available for that deployment.

The data obtained from the instrumented frames were augmented with vertical profiles collected from the centre of the channel at each station using a LISST and a SeaBird CTD. Additionally, surface water samples for nutrients, pathogens, and SPM were collected. Water samples and profiles were obtained every 15–30 min for up to 12.5 h per day over two consecutive days during spring tides at the start and end of each moored instrument deployment.

Further, the instrumented bed frames were deployed over a lunar cycle in October 2017. For this deployment, three frames were positioned across the channel at Station 1 (Tal-y-Cafn) near the west margin, centre of the channel, and east margin. The purpose of these deployments was to examine the dynamics of the axial convergent front.

2.3. SPM calibration

On each deployment, water samples were collected for the gravimetric determination of SPM mass concentration, which was used to calibrate the LISST transmissometers and ADCPs. For gravimetric determination, 1 l of water was filtered onto pre-ashed and weighed Whatman GF/F filters with a nominal pore size of 1.2 mm. Following the filtration, the filters were dried in an oven for an hour at 75 °C, and then re-weighed after a period of cooling in a desiccator. Three blank filters were also analysed to account for potential bias. Additionally, within each batch, one sample (separated into approximately 300 ml portions) was filtered onto three separate filters to assess measurement error.

SPM mass concentration profiles were computed from the ADCP backscatter signal calibrated using the measured SPM concentrations derived from the collected samples at each deployment. The method has been described by Deines (1999), Ha et al. (2011), Ho and Park (2012). The mass concentration C_m was obtained by:

$$10\,log_{10}\,(C_m) = C_k + 10\,log_{10}\,(r^2) + 2\alpha_w\,r + K_c\,E \quad (1)$$

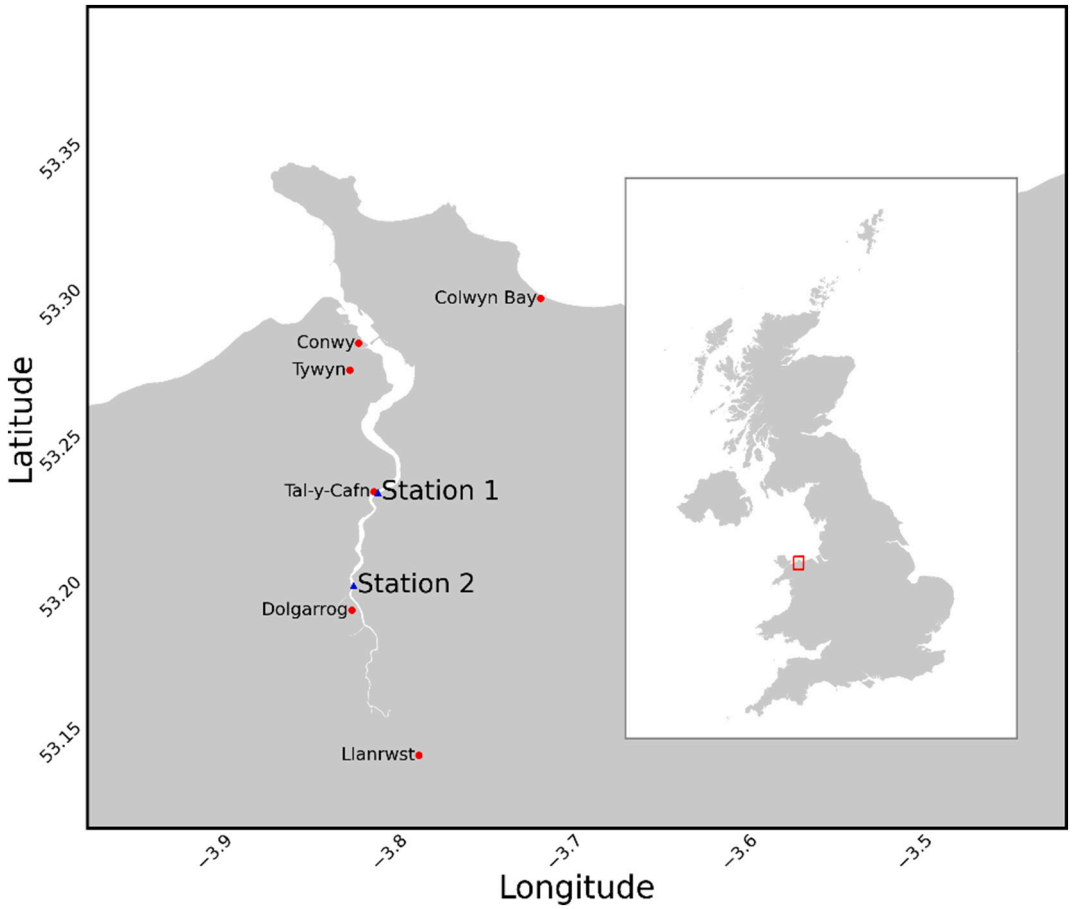

Fig. 1. The Conwy River and Estuary in North Wales, west UK (inset), showing observation stations at Tal-y-Cafn (Station 1) and Dolgarrog (Station 2).

where C_k is a constant, r is the sensing range, α_w is an attenuation coefficient, K_c is the received signal strength indicator scale factor, and E is echo strength (in counts). For a 1200 kHz ADCP α_w is typically taken as 0.48 dB m^{-1}. The two calibration constants, C_k were and K_c, were determined by linear regression using backscatter data and measured mass concentration from water samples for each deployment.

2.4. E. coli and total coliform enumeration

The FIOs *E. coli* and total coliforms were analysed according to protocols described within Hassard et al. (2017). Autoclave-sterilised glass bottles were used to collect duplicate water samples prior to *E. coli* and Coliform enumeration. Samples were collected by immersing each bottle beneath the water surface in the direction of flow. The collected samples were refrigerated by storing on melting ice initially and returned to the lab for refrigeration and subsequent analysis within 8 h of collection. Enumeration was performed using the membrane filtration method. Water samples were homogenized by shaking, following a $\log_{10}$ dilution series. Then, 10–100 ml of water sample was filtered under vacuum using sterilised equipment through a 0.2 μm cellulose nitrate membrane (Sartorius, Germany). The membranes were aseptically transferred to inoculate solid agar selective medium for the enumeration of *E. coli* and coliforms (Harlequin *E. coli* / Coliforms Media, Lab M, UK). Averages were calculated of the appropriate dilutions considering triplicate method replicates (ISO 9308-1, 1990). The plates were then incubated and enumerated following manufacturer recommendations. The detection limits for culturable bacteria were estimated using serial dilution, reaching down to 1 CFU/100 ml for the water samples.

2.5. Macronutrients

To minimise contamination of nutrients from external sources, all glassware was cleaned to render it organic-nutrient free. The cleaning procedure followed the method described in Standard Methods (Eaton and Franson, 2005). First, 40 ml borosilicate vials were washed with detergent followed by rinsing three times with ultrapure (UP) water. These vials were soaked in 0.2 M hydrochloric acid (HCl) overnight before being rinsed another three times with UP water. The vials were then capped with aluminium foil and heated in a muffle furnace at 550 °C for 6 h to remove any traces of organic matter. Surface water samples were collected from the middle of the estuary at Station 1 and Station 2. The sampling bottle was rinsed with estuary water before filling with the final sample. The sample was returned to the laboratory on the same day and stored at 4 °C until processing, which took place within two days.

The collected sample was decanted into nutrient free measuring cylinders and subsequently vacuum filtered. Up to 500 ml of sample were filtered over each filter. Two filters, each placed in separate filter housing, were utilised for different analyses, one per filter housing. A 0.45 μm cellulose nitrate filter was used for Total Phosphorus (TP) analysis and a pre-ashed Whatman GF/C was used for Total Carbon (TC) and Total Nitrogen (TN). The following analyses focused on the particulate (thus suspended) fractions of the SPM. The soluble constituents for each nutrient were also quantified, but the data are not reported here.

The volume of each sample was recorded, and the filters were oven dried overnight at 105 °C and subsequently allowed to cool in a desiccator. The following water constituents were then determined for TC, TN and TP. For TC, total organic and total inorganic fractions were determined via Standard Method using a TOC-V Analyser (Shimadzu, Japan). For TC, both the total organic and total inorganic fractions were determined using Standard Method 5310 TOC (American Public Health Association, APHA, 2018a) with a TOC-V Analyzer (Shimadzu, Japan). The organic carbon content was calculated by measuring the total carbon (TC) and inorganic carbon (IC). The TN was determined by oxidative digestion of all digestible nitrogen forms to nitrate, followed by quantification of the nitrate by colorimetry, according to Standard Method 4500-N C (APHA, 2018b). The TP was analysed from each water sample following the acid/heat digestion and colorimetry approach described in Standard Method 4500-P (APHA, 2018c). These values, obtained from the filtered material, represent the particulate components of the macronutrient pool.

2.6. Turbulent dissipation rate

The turbulent dissipation rate, ε ($m^2\ s^{-3}$), was calculated using the structure function method (Wiles et al., 2006). The second-order structure function, D (r, d), is given by:

$$D(r,d) = \overline{(v'(r) - v'(r+d))^2} \quad (2)$$

where v' is the ADCP beam velocity minus its temporal mean, r is the range along the beam and d is the distance between two points along the beam. Kolmogorov's 2/3 law then relates $D(r, d)$ to ε such that:

$$D(r,d) = C_v \varepsilon^{2/3} d^{2/3} \quad (3)$$

where C_v is a constant (= 2.0; Rusello and Cowen, 2010).

2.7. Statistical analysis

To understand the potential correlations between particle size classes, macronutrients, and pathogens, Pearson's correlation coefficient was calculated. This analysis was conducted using the statistical software SPSS (v25.0.0.0, IBM, UK). Values were corrected using multiple comparisons to avoid type I errors using the Bonferroni correction.

3. Results

3.1. Hydrodynamics

ADCP data at Station 1 (Tal-y-Cafn) during all deployments exhibited a time-velocity asymmetry, an established characteristic of the Conwy and other shallow macrotidal estuaries as described in prior studies (e.g., Allen et al., 1980; Jago, 1980; Dronkers, 1986; Uncles and Stephens, 1993; Brenon and Le Hir, 1999; Jago et al., 2006b; Chernetsky et al., 2010; Yu et al., 2014). This asymmetry was characterised, on spring tides, by a faster, shorter flood tide, lasting approximately 2.75 h with flows reaching about 1 m s^{-1}, and a slower, longer ebb tide, lasting about 9.5 h with flows reaching about 0.8 m s^{-1} (Fig. 2A). Interestingly, while the flood velocities were 20–30 % faster than the ebb velocities, measurements of turbulence dissipation presented a tidal asymmetry that was ebb-dominant (Fig. 2B). Turbulence dissipation rates peaked at $1 \times 10^{-4}\ m^2\ s^{-3}$ in the lower few metres of the water column during both flood and ebb tidal phases. However, these values extended throughout the water column during the ebb but were dampened to approximately $1 \times 10^{-5}\ m^2 s^{-3}$ in the upper waters during the flood. Therefore, when averaged vertically, the peak flood turbulent dissipation rates were 10–50 % weaker compared with the ebb. This phenomenon at Tal-y-Cafn was regularly observed during the observational periods (Fig. 2C and D). This ebb-dominant turbulence asymmetry was not observed on neap tides (Fig. 6B).

The observed shift from a flood-dominant asymmetry in tidal velocities to ebb-dominant asymmetry of the turbulence field aligns with the preliminary findings presented within Howlett et al. (2015). They attributed this change to a tidal straining process linked with an axial convergent front, first recognised by Nunes and Simpson (1985). The front signifies surface convergence, which stems from the interaction of bathymetry, cross-channel shear of the along-channel current, and the along channel salinity gradient (Turrell et al., 1996). During the flood tide, the velocity is higher in the deeper central part of the estuary than

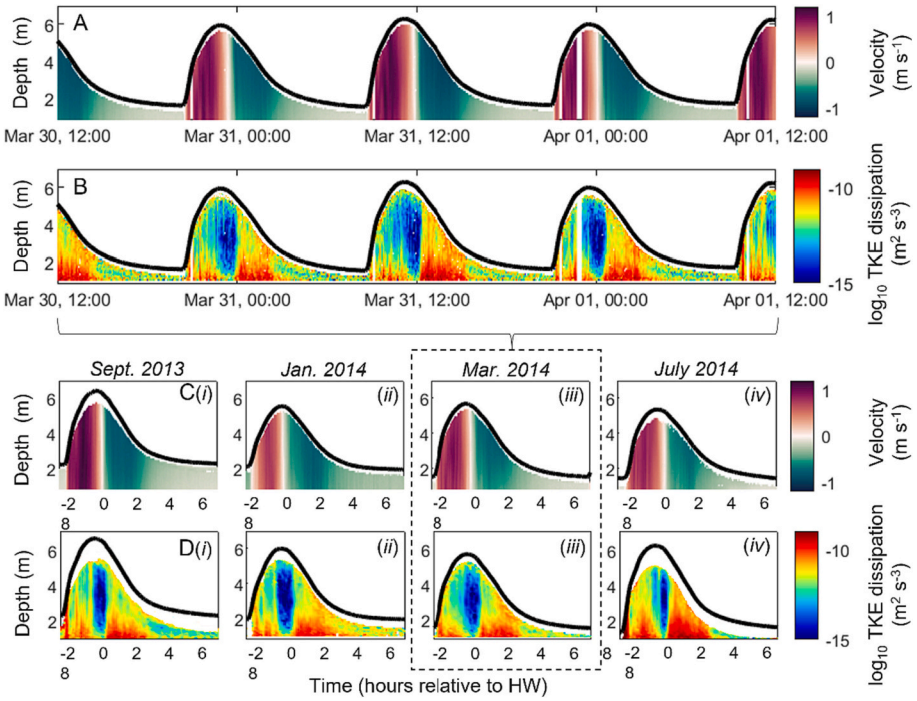

Fig. 2. Station 1 (Tal-y-Cafn): ADCP measurements during four successive tidal cycles (March–April 2014), illustrating (A) along-channel velocities (m s^{-1}, positive values indicate upstream direction during the flood tide), and (B) the corresponding along-channel turbulent kinetic energy (TKE) dissipation rate (m^2 s^{-3}) presented on a log10 colour scale. Panels (C) and (D) depict along-channel velocity and log10 TKE dissipation rate, respectively, during the spring tidal cycles in (i) Sept. 2013, (ii) Jan. 2014, (iii) Mar. 2014, and (iv) July 2014. Data in (i–iv) are displayed in phase-averaged form relative to high water (HW), with averages taken over four spring tidal cycles; for instance, the data in A and B have been averaged to produce C(iii) and D(iii), respectively. The black line in all panels indicates the water depths (m).

at the shallower margins, causing salinity to rise faster in the centre than at the margins. This condition creates a lateral salinity gradient, which in turn generates cross-channel currents which have previously been measured to reach approximately 0.2 m s^{-1} at the surface, or ~20 % of the along-channel flows (Turrell and Simpson, 1988; Brown et al., 1991). The lateral currents converge towards the (approximate) channel centre from the margins, leading to a frequently observed surface slick and aggregation of spume and flotsam. The convergence brings waters from the margins, that have slower along-channel velocities, to the centre which alters along-channel current shear and permits the temporary development of stratification. This is indicated by an increased potential energy anomaly indicative of stratification in the upper part of the water column (see Supplementary Material, Fig. S5) which, in turn reduces observed turbulence. The disappearance of the ebb-dominant turbulence asymmetry on neaps is due to the reduction of lateral currents and resultant stratification on the flood tide because along-channel currents and lateral salinity gradients are considerably diminished.

To describe in more detail the axial convergence at Tal-y-Cafn, the three ADCPs deployed in autumn 2017 across the channel are shown in Fig. 3. The data within these figures distinctly demonstrate surface convergence during the late flood tide and surface divergence during the early ebb tide (Fig. 3A–E). The surface lateral flows reached ~0.25 m s^{-1} during spring tides, representing approximately 25 % of the along-channel flow (Fig. 3C–E). The convergent/divergent flows weakened towards the bed and sometimes reversed direction (e.g., Fig. 3F). This pattern was generally repeated during every tidal cycle of the 20-day deployment, except for a period of heavy rain and strong river discharge from October 13 to 15 (refer to Supplementary Material, Figs. S2–S3). As Howlett et al. (2015) demonstrated, this cross-channel circulation transports water with a slower along-channel velocity towards the centre of the estuary at the surface, thereby slowing the surface layer and generating a subsurface jet with peak velocity at mid-depth.

By contrast, at Station 2 (Dolgarrog), both flood-dominant velocity asymmetry and flood-dominant turbulence asymmetry were observed (Supplementary Material, Fig. S4), even during instances of significant saltwater penetration on spring tides. This pattern emerges because the channel at Dolgarrog is too narrow (~30 m) to support the development of substantial transverse currents, thereby preventing the flood stratification/turbulence damping observed at Tal-y-Cafn. Consequently, a shift in turbulence asymmetry occurs within the RETZ between Stations 1 and 2, which are approximately 5 km apart.

3.2. SPM properties

SPM mass concentration, volume concentration, and size spectra are shown for the 2013/2014 surveys at Tal-y-Cafn and Dolgarrog, in Fig. 4, respectively. Notably, significant peaks in SPM mass concentration at both sites correspond to rapid current speeds during the flood and ebb tides, showing local resuspension. However, other peaks seen earlier in the flood and later in the ebb do not correspond with current speed, indicating the presence of advecting horizontal concentration gradients.

At Station 1 (Tal-y-Cafn) (Fig. 4A–C), taking the September 2013 deployment as an example, increases in SPM mass concentration coincided with fast flood and ebb currents. However, the concentrations peaked (up to 100 g m^{-3}) earlier in the tidal cycle than the maximum current speeds (Fig. 4B(*i*)). This is a common observation where there is a finite supply of easily-suspended matter on the bed. The minimum concentration and maximum median particle size (400 μm) were observed briefly at slack high water, indicative of aggregation and settling under low turbulence conditions (Fig. 4C(*i*)). The median size of resuspended material was greater on the ebb tide (100–200 μm) than on the flood tide (50–100 μm) (Fig. 4C(*i*)). In addition, there were advective SPM mass and volume concentration peaks (>100 μl l^{-1}) on the early flood and the late ebb tide, coinciding with the arrival and departure of saltwater (Fig. 4A(*i*)). The early flood SPM concentration peak, which

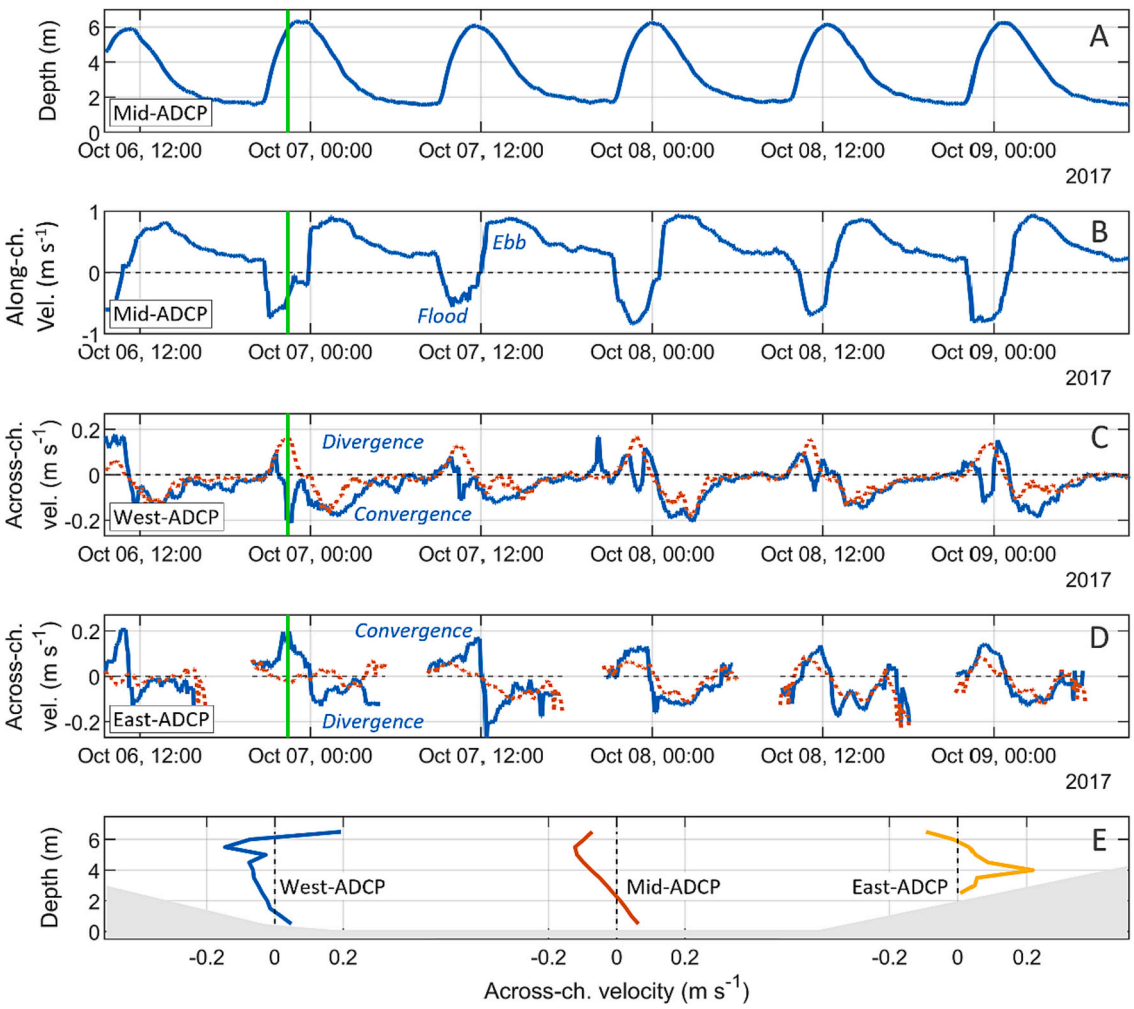

Fig. 3. Station 1 (Tal-y-Cafn): Demonstrates the evidence of axial convergence from three ADCP deployments during 06–09 October 2017. Panel (A) presents a timeseries of mid-channel water depths, and panel (B) displays timeseries of longitudinally-resolved surface velocities (positive values indicate ebb flow). Timeseries of laterally-resolved surface velocities (blue curves) and bottom velocities (orange dotted curves) are displayed for west- (C) and east-channel (D) ADCP deployments (positive values indicate northwest directed flows). Panel (E) illustrates the instantaneous velocity vectors at each depth bin through a west-east transect at Tal-y-Cafn at 22:25 on October 06 (indicated by the horizontal green line in panels A-D). Positive values indicate southeast directed flows. The pattern shown was consistent throughout the ADCP deployments from October 06 to 20, 2017, except during periods of large river flows (see Supplementary Material, Figs. S2-S3).

had a median size of 100 μm, was on the cusp of the advancing saltwater, lasted approximately 15 min, and had passed the surveillance station before resuspension of the bed material began. A high concentration of very large flocs (with a median size of 200–300 μm) was seen in a late ebb turbid cloud, occurring 3–4 h after resuspension has ceased, and was independent of the local hydrodynamics. These characteristics were observed during three of the four periods of observation (Sept. 2013, Mar. 2014, July 2014) but were muted in January when there was reduced upstream salinity penetration due to larger freshwater discharge (20–74 $m^3 s^{-1}$).

At Station 2 (Dolgarrog) (Fig. 4D–F), using September 2013 as an example deployment, increases in SPM concentration (up to 200 g m^{-3}) corresponded with rapid flood and ebb currents (Fig. 4E(*i*)), a similar trend to that observed at Tal-y-Cafn, indicating resuspension of material from the bed. The minimum concentration and largest median size (400 μm) coincided with high slack high water suggesting aggregation and settling under low turbulence (Fig. 4F(*i*)). As at Tal-y-Cafn, the resuspended material at Dolgarrog had a larger median size on the ebb tide (200–300 μm) than on the flood tide (50–100 μm) (Fig. 4F(*i*)). Advection of SPM, coinciding with the arrival of a small amount of saltwater (observed on spring tides only); carried material with a median size of 100 μm (Fig. 4F(*i*)), matching the size of advected material at the forefront of the advancing saltwater at Tal-y-Cafn. High concentrations of large flocs (>100 μl l^{-1}) were observed as the saltwater exited the station after ebb velocities declined. These large flocs (with a median size of 200–300 μm) continued to advect past the site for nearly 2 h after the departure of saltwater, showing that they originated from upstream in the tidally influenced river (Fig. 4F(*i*)). This material continued to move downstream at approximately 0.4 m s^{-1}, reaching Tal-y-Cafn about 2 h later. The main features of the SPM signal were observed during the three periods of observation (Sept. 2013, Mar. 2014, July 2014) for which we have good data.

3.3. Particulate nutrients and pathogens

The time series data displays Chlorophyll and SPM mass concentrations relative to concentrations of particulate carbon, nitrogen, phosphorus, and faecal indicator organisms (surrogate for pathogens) over multiple tidal cycles during October 2013 at Station 1 — Tal-y-Cafn (Fig. 5). Two peaks in Chlorophyll and SPM mass concentrations were evident during the flood tide, initially due to the advancing ETM and then due to local resuspension of SPM during peak mid-flood currents. Similarly, two peaks in Chlorophyll and SPM mass concentrations were evident during the ebb tide, initially due to resuspension of the local bed

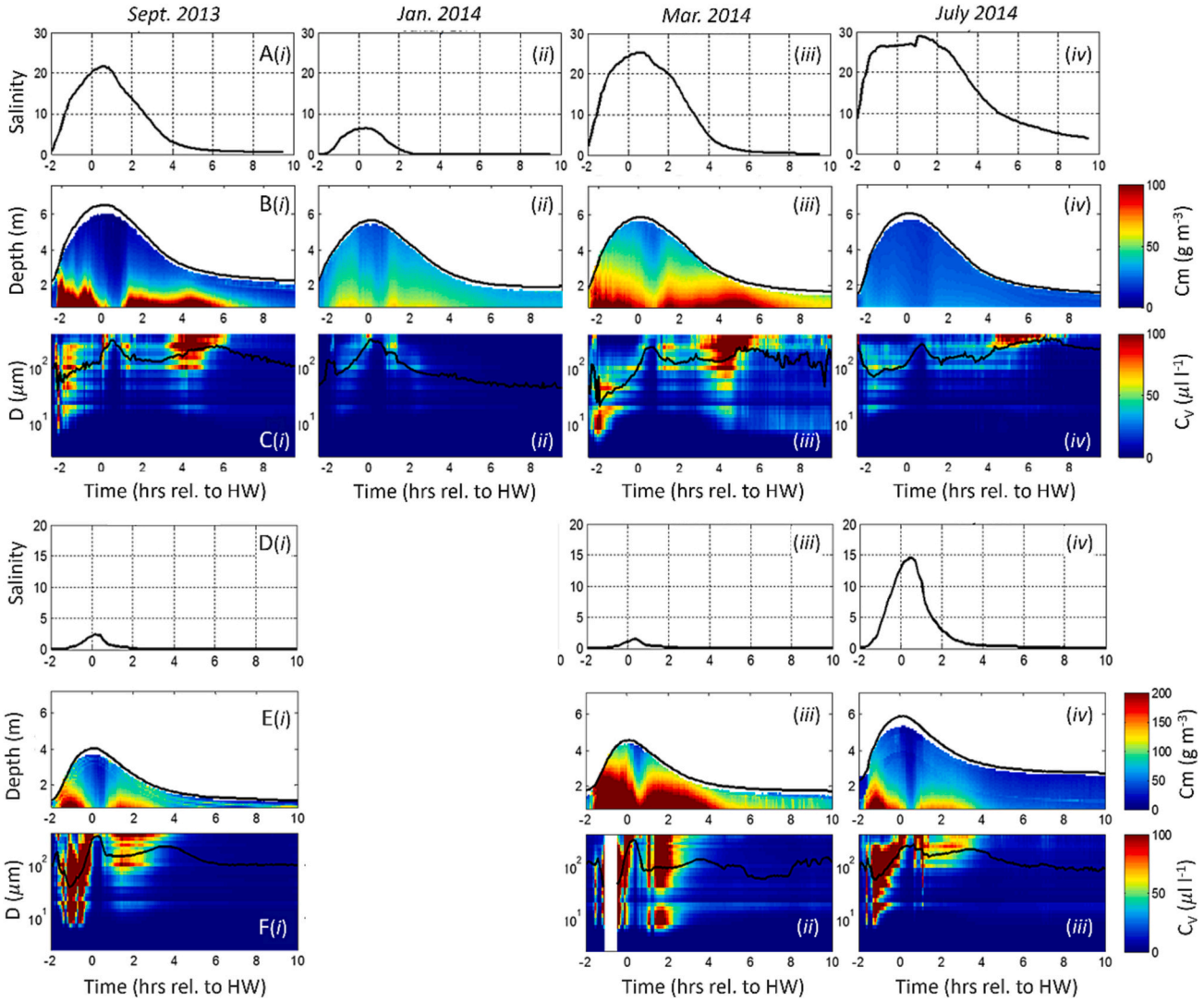

Fig. 4. Rows (A–C) display measurements at Station 1 (Tal-y-Cafn), showing (A) salinity, (B) SPM mass concentration (C_m), and (C) volume concentrations of particle size spectra (C_V), during the four sampling periods: (i) Sept. 2013, (ii) Jan. 2014, (iii) Mar. 2014, and (iv) Jul. 2014. The particle size spectra also present the median particle size D_{50} (black line). The data represent averages taken from four successive spring tides. Corresponding measurements for Station 2 (Dolgarrog) are shown in rows (E-F) during three sampling periods: (i) Sept. 2013, (ii) Mar. 2014, and (iii) Jul. 2014. The data for the Jan. 2014 sampling period was found to be erroneous and is therefore not shown.

material and later as the ebb ETM advanced downstream. Slightly larger tides on the 6th October than on the 5th (tidal range increased from 7.1 m to 7.8 m), and weaker river flows (daily mean discharge decreased from 10 $m^3 s^{-1}$ to 7 $m^3 s^{-1}$) likely caused the increased Chlorophyll and SPM mass concentrations on the second day. The ratio of Chlorophyll (land sourced) to SPM mass concentration roughly indicates the stage of the tidal cycle, with the ratio increasing during the onset of flood tide and peaking during the late ebb tide. The particulate nutrient and pathogen data are of lower temporal resolution and exhibit more noise compared with SPM. The most prominent peaks in particulate nutrients and pathogens are observed corresponding to the arrival of SPM at the beginning of the flood tide and the resuspension of SPM during the mid-flood, and aligning with the advecting SPM turbid cloud (ETM) during the late ebb tide. On the ebb tide, the highest recorded concentration of *E. coli* reaches 2500 CFU/100 ml. For comparison, a minimum of 500 CFU/100 ml *of E. coli* was consistently detected on the rising limb of the flood tide, likely attributed to the migration of the turbid SPM cloud.

4. Discussion

4.1. SPM dynamics

The advancing flood tide transports turbid, saline water from the lower estuary's intertidal flats, towards RETZ (Station 1, Tal-y-Cafn). Our results show that the SPM in this region consists of flocs of a median size of about 50 μm. This phenomenon creates an estuarine turbidity maximum (ETM) at the leading edge of the saltwater intrusion, comprised of low-density aggregates. The solitary ETM forms and fragments during each flood and ebb phase of the tide. Previous studies in the Conwy have illuded to this phenomenon but noted further observations were required (e.g., West et al., 1986; West and Sangodoyin, 1991). In comparable macrotidal estuaries, a similar mechanism for the formation of an ephemeral ETM composed of organic-rich, low-density aggregates has been observed (e.g., Jago et al., 2006a). Once the SPM spike has passed Tal-y-Cafn, the mass concentration of SPM decreases. However, as current speeds increase during the mid-flood tide, local resuspension occurs, temporarily increasing the SPM mass concentration before declining due to depletion of the particle supply.

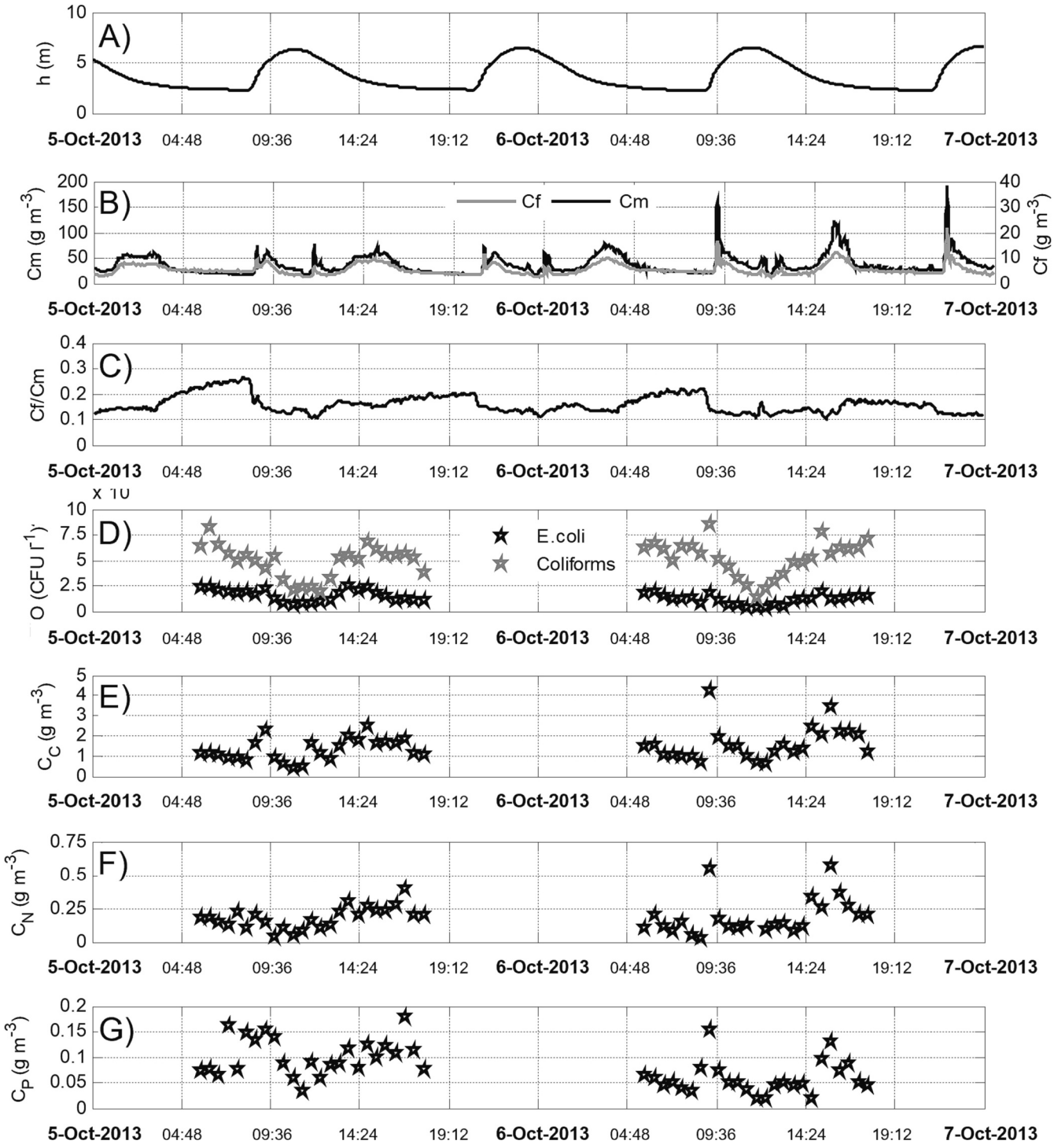

Fig. 5. Station 1 (Tal-y-Cafn), presenting data from four consecutive tides in October 2013, including: (A) water level; (B) chlorophyll (C_f) and SPM mass concentration (C_m); (C) chlorophyll/SPM mass concentration ratio; (D) particulate concentrations of faecal indicator organisms (FIOs) for *E. coli* and coliforms; (E) particulate carbon concentration (C_C); (F) particulate nitrogen concentration (C_N); and (G) particulate phosphorus concentration (C_P).

At the upstream end of the RETZ (Station 2, Dolgarrog), the increasing flood tide currents reverse the flow of the freshwater river before the arrival of the ETM (about 1.5 h after the ETM has passed Tal-y-Cafn). The ETM at Dolgarrog exhibits similar concentrations and median size compared with Tal-y-Cafn. The median size of particles in the advecting ETM is smaller than in the locally resuspended component.

During slack high water at both Tal-y-Cafn and Dolgarrog, aggregation occurs under low turbulence conditions, leading to the formation and deposition of larger flocs. This process results in a significant decrease in SPM mass concentration at both sites. The flood-generated ETM which is now landward of Station 2 must also similarly decline. Ebb currents then induce resuspension at both sites, with Dolgarrog experiencing a more significant resuspension compared with Tal-y-Cafn. The most prominent SPM signal is a newly formed ebb generated ETM, characterised by aggregation and resuspension upstream of Dolgarrog. This ETM, consisting of flocs with a median size of 200–300 μm, is advected downstream from the tidally influenced river and reaches Tal-

y-Cafn about 2.5 h later. Peak SPM concentrations are higher at Dolgarrog than at Tal-y-Cafn, which can be partly attributed to concentration effects as the channel width widens downstream. Furthermore, the median size of SPM in the ebb ETM is greater than in the flood ETM.

The ebbing ETM then passes into the main body of the estuary and is either deposited on the emerging intertidal sand flats or is flushed from the estuary into the nearshore zone. A new ETM is then regenerated by the next advancing flood tide. Hence it is an ephemeral feature which is created and destroyed with every tide. This study focused on periods of spring tides with generally low river discharge – it must be noted therefore that these processes would be expected to shift seaward during neap tides (25–30 % weaker tidal flows), and/or during high river discharge, in accordance with the shifting ETM (indeed the saline intrusion does not reach Station 2 during neaps).

4.2. SPM flux

Our study allows for the interpretation of net suspended particulate matter (SPM) mass fluxes along the estuary. To calculate these fluxes, initially we used velocity and SPM mass concentration time series data obtained from calibrated ADCP profiles at the mid-estuary (Station 1, Tal-y-Cafn) and upper-estuary (Station 2, Dolgarrog) locations where the instruments were deployed in 2013/2014. Specifically, these measurements were taken at the centre of the channel width. When we summed the values vertically and over the four tidal cycles during the March 2014 survey (Fig. 7), we found a net SPM mass flux of 7 kg m^{-1} $tide^{-1}$ seaward at Tal-y-Cafn and 70 kg m^{-1} $tide^{-1}$ landward at Dolgarrog. This pattern of net divergence in SPM mass flux between the two stations was also observed in the September 2013 and July 2014 surveys, although data for the January 2014 survey were not available. The net seaward (ebb) SPM mass flux at Tal-y-Cafn disappeared during neap tides when there was a small net landward (flood) flux (Fig. 6D).

Since the above calculations were based on a single mooring in the centre of the channel and, considering the significance of transverse circulation at Tal-y-Cafn, we also calculated SPM mass fluxes using data from the three ADCPs distributed across the channel at Station 1 during October 2017 (Fig. 8). During periods of low river flow conditions (<50 m^3 s^{-1}), the net SPM flux at the mid-channel mooring was comparable to the previously calculated values (<100 kg m^{-1} $tide^{-1}$ seaward). This pattern was repeated, albeit with smaller fluxes, for the moorings closer to the banks, giving us confidence that these patterns are representative of the full channel width. By integrating these SPM fluxes from the three moorings across the channel, assuming the depth at each ADCP represents one third (40 m) of the channel width (120 m), the channel-averaged net SPM mass flux was seaward at $<6 \times 10^4$ kg $tide^{-1}$. However, the flux substantially increased during a high discharge event on 15th October when the river discharge reached 340 m^3 s^{-1} (a >99th percentile event). During this event, the seaward SPM flux increased to 2×10^4 kg m^{-1} $tide^{-1}$ at the central mooring and 1×10^6 kg $tide^{-1}$ when integrated across the three moorings. Hence one river flood event generated a seaward flux past Station 1 that was two orders of magnitude greater than the seaward flux during low river flow conditions.

To gain further insights into SPM fate and transport and role of the RETZ, we investigated volume fluxes for discrete particle sizes using the particle size data obtained from the LISST during the March 2014 survey. The results for both stations are presented in Fig. S6. At Station 2 (Dolgarrog), the net volume flux of flocs within the range of 10–100 μm was directed landwards, with minimal flux observed for smaller and larger particles. High SPM concentrations at Station 2 during peak flow were due to local resuspension of material rather than suspended sediments advancing from up/downstream. This pattern aligns with the landward mass flux observed in Fig. 7. These findings are consistent with sediment transport dynamics in shallow, macrotidal estuaries where tidal pumping transports sediment landwards (Allen et al., 1980; Jago, 1980; Uncles and Jordan, 1980; Uncles et al., 1985). By contrast, at Station 1 (Tal-y-Cafn), the depth-averaged net volume flux was negligible but displayed a seaward direction near the bed for flocs larger than 200 μm during two out of the three tides. It was these larger flocs that

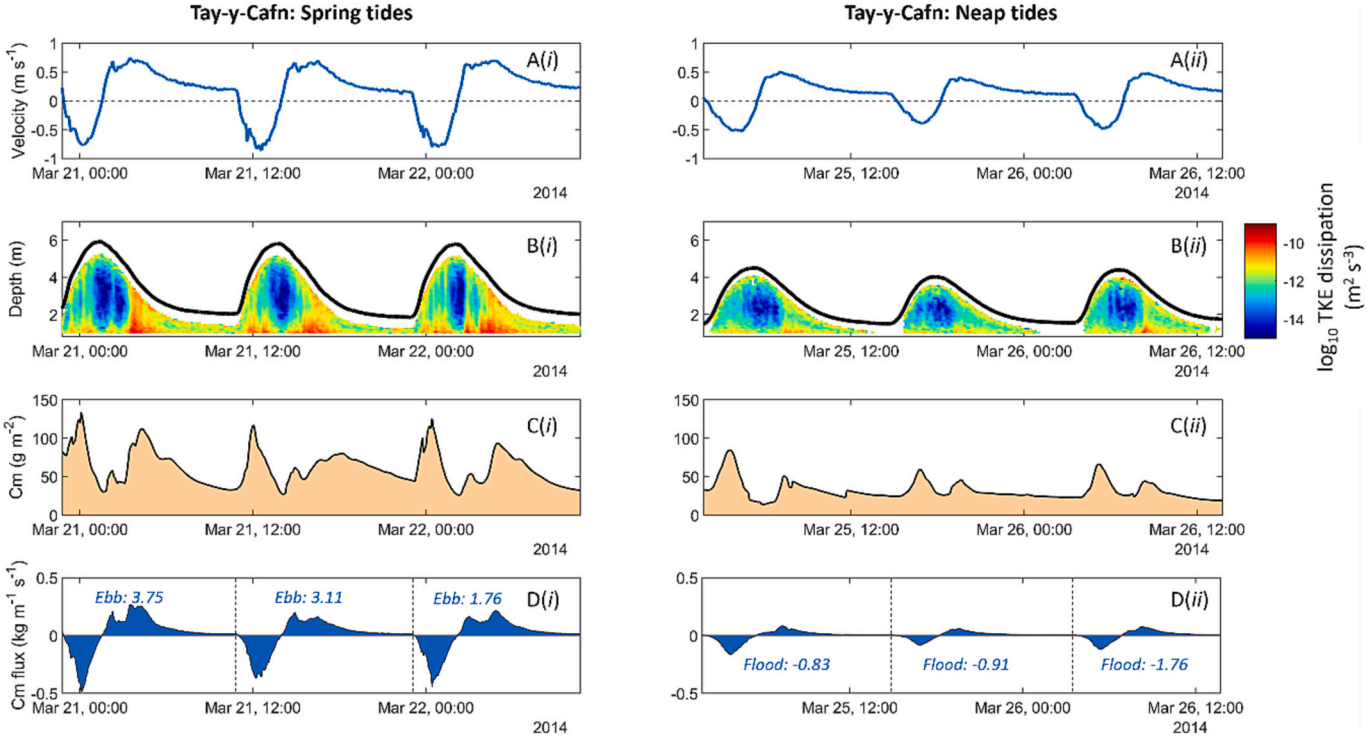

Fig. 6. Station 1 (Tal-y-Cafn) during March 2014: (A) Depth-averaged along-channel velocity (m s^{-1}); (B) $\log_{10}$ TKE dissipation rate (m^2 s^{-3}); (C) depth-integrated SPM mass concentration (g m^{-2}); and (D) SPM mass flux (kg m^{-1} s^{-1}). The left panels (i) show the data during three spring tidal cycles whereas the right panels (ii) show the data during three neap tidal cycles. In (A) and (D), positive values indicate the ebb tide (up-estuary) direction.

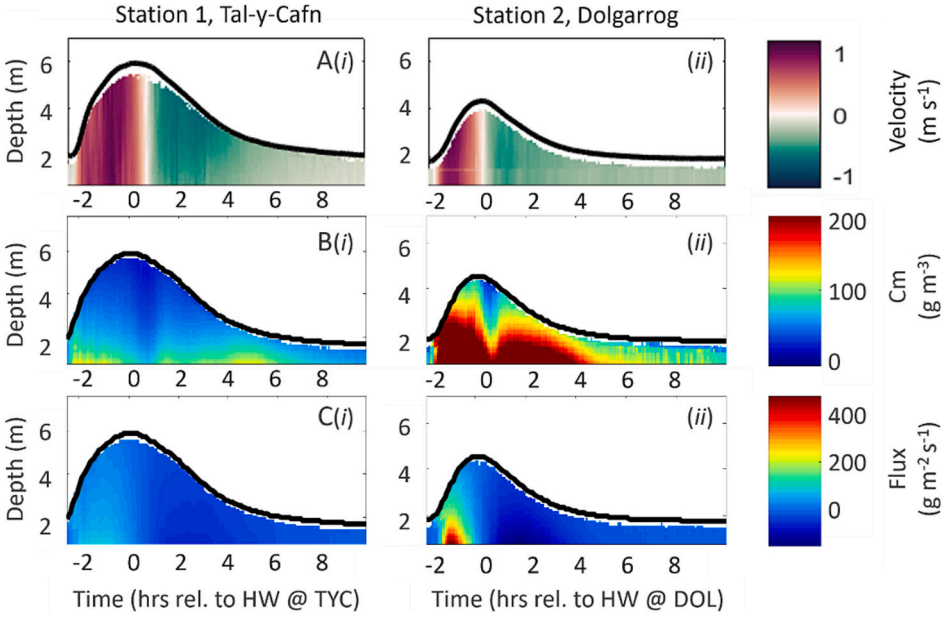

Fig. 7. (A) Averages over four spring tides during March 2014 showing (A) along-channel velocity (m s^{-1}), (B) SPM mass concentration (g m^{-3}), and (C) SPM mass flux (g m^{-2} s^{-1}) at (i) Station 1 (Tal-y-Cafn) and (ii) Station 2 (Dolgarrog). Positive values indicate flood tide (up-estuary) direction.

primarily contributed to the seaward mass flux observed at this station.

The absence of net landward transport at Station 1 (Tal-y-Cafn) was unexpected and can be attributed to the reversed turbulence asymmetry observed. The reduced turbulence on the flood tide inhibits the resuspension of sediment and hampers the dispersion of SPM into faster-flowing waters. This effect is particularly significant for larger flocs, which require more turbulence energy to be transported away from the near-bed region. Consequently, the depth-integrated flux of SPM is reduced, resulting in a decrease in the flood flux on the flood tide. However, on the ebb tide, when turbulence is fully developed, the net flux of large flocs seawards is observed, presenting a contrasting behaviour to the tidal pumping seen at Station 2.

An intriguing and unexpected consequence of the observed dynamics is the selective transport of flocs within specific size ranges. Flocs ranging from 10 to 200 μm are pumped landward into the tidally influenced river above Dolgarrog, resulting in their confinement within this region. Conversely, flocs larger than 150 μm are exported seaward from Tal-y-Cafn, bypassing the RETZ. This process leads to a particle size fractionation of SPM within the estuary, where different size fractions exhibit distinct transport patterns. During periods of strong river discharge, however, net SPM fluxes are directed seawards at both stations.

4.3. Particulate nutrients and FIOs

We examined the distribution of particulate nutrients and FIOs in the particle size spectrum of SPM from the 2013/14 surveys. Correlation coefficients (R^2) were determined between the gross nutrient/FIO concentration and the individual volume concentration for each particle size class determined by the LISST ($N = 32$ classes). These analyses, based on data from all samples taken at Station 1 (Tal-y-Cafn) throughout the 2013/14 seasonal campaign, consistently showed high, statistically significant R^2 values for particle sizes in the range of 10–200 μm. However, particles smaller than 10 μm and larger than 200 μm showed low R^2 values that were not statistically significant (Fig. 9).

The correlation of nutrient/FIO concentration with intermediate size flocs is indicative of their importance for biogeochemical fluxes. However, there was no correlation between nutrient/FIO concentration and the concentration of very small or very large flocs. This suggests that the key flocs for biogeochemical processes are those of intermediate size rather than very large flocs. Our findings also suggest that there is a compositional equilibrium within the 10–200 μm flocs, which is expected in mature flocs where nutrients have transferred from dissolved to particulate phases and FIOs have accumulated. In contrast, the larger flocs formed in the ETM are relatively young and have not had enough time for nutrients and FIOs to increase in proportion to their increased size. Because of their loose structure, large flocs are bigger than the sum of their original components. But the nutrient/FIO content is initially exactly the sum of the original components. The R^2 values thus could serve as useful proxy for floc age in estuarine systems.

During periods of increased resuspension, the microbial water quality in the Conwy estuary often exceeded regulatory thresholds. For example, 94 % of water samples tested at Station 1 exceeded the bathing water standards set by EU and UK regulators. There are several possible sources of the poor water quality, including agricultural run-off, combined sewer overflows (CSOs), wastewater treatment works, and wild animals and autochthonous inputs (Hassard et al., 2017). These standards aim for “excellent” water quality status and specify limits of 250 CFU/100 ml for *E. coli* in coastal and transitional waters, and 500 CFU/100 ml for inland waters. The peak value for *E. coli* in this study was approximately 20 times higher than the inland water standard. It is important to note that the study’s findings challenge the current monitoring practices, which do not consider tidal status. Clearly, SPM and FIO concentrations change dramatically by the hour in the RETZ of the Conwy estuary. As a result, decision makers, or increasingly the public, may have access to misleading data when assessing water quality and making management decisions. While this study focuses on the Conwy estuary, and only two locations within it, conducting comparative analyses with other estuaries could provide further insights into the uniqueness or generalizability of the observed patterns and processes. Additionally, future studies could incorporate spatially diverse observations and estuary-wide model simulations.

5. Conclusions

The river-estuary transition zone (RETZ) of the shallow macrotidal Conwy estuary (UK), under low river flow conditions, was found to be a conduit for SPM rather than a zone of accumulation, with complex size fractionation and biogeochemical exchanges of particulate nutrient/FIO compositions. This novel result adds to previous understandings of

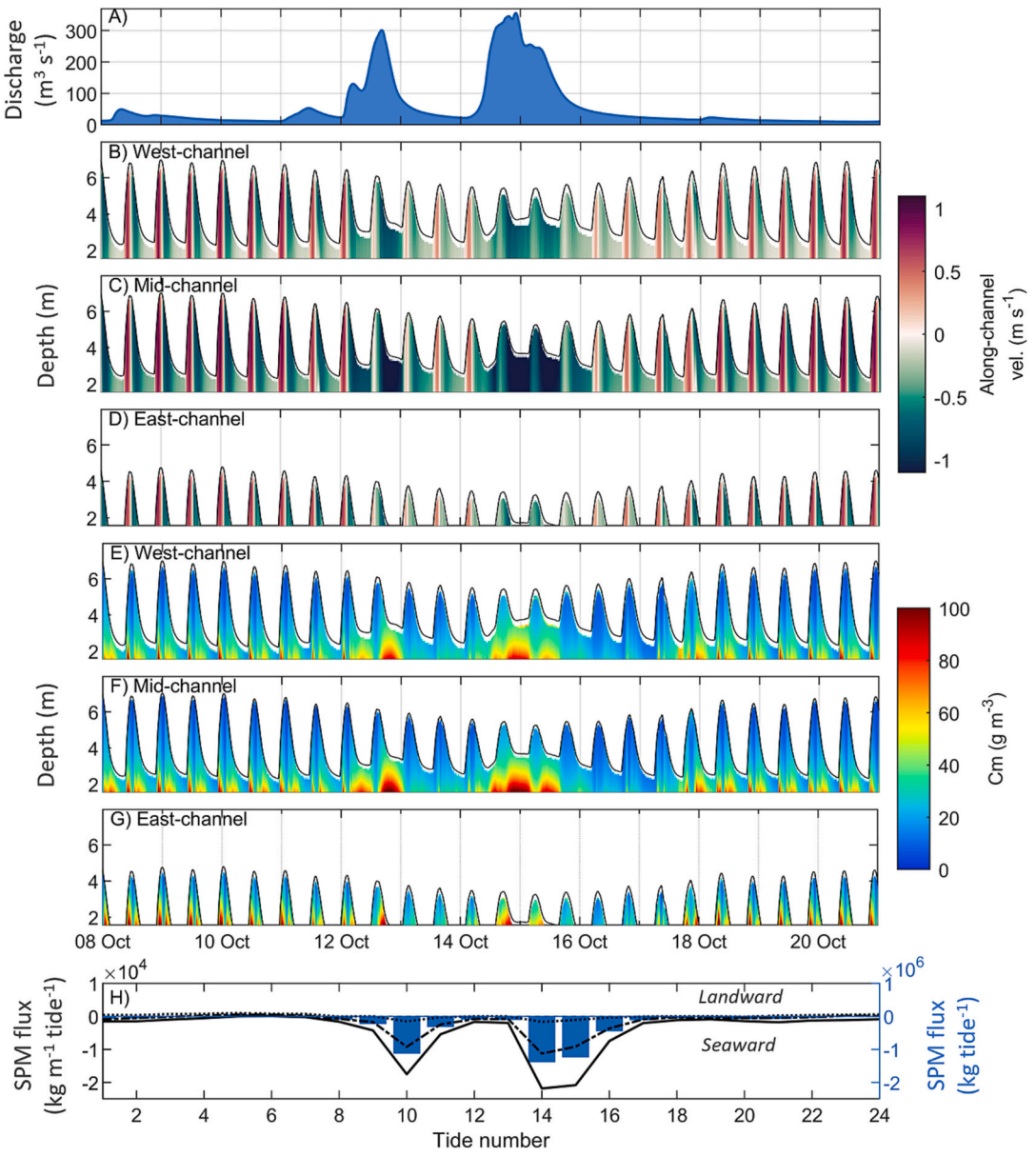

Fig. 8. Station 1 (Tal-y-Cafn) during the survey in October 2017: (A) River Conwy discharge ($m^3\ s^{-1}$); (B–D) Along-channel velocity ($m\ s^{-1}$)at the west/mid/east moorings; (E-G) SPM mass concentration ($g\ m^{-3}$) at the west/mid/east moorings; and (H) depth- and tide-averaged SPM flux ($kg\ m^{-1}\ tide^{-1}$) for the west (dot-dash line), mid (solid line) and east (dotted line) moorings (left y-axis), and depth-, width-, and tide-averaged SPM flux ($kg\ tide^{-1}$) assuming each mooring represents one third (40 m) of the channel width (120 m) (right y-axis).

estuary SPM dynamics (e.g., see Burchard et al., 2018). Measurements of the hydrodynamics, SPM dynamics, and particulate biogeochemistry of the RETZ showed large variations on tidal and seasonal time scales.

In the lower part of the RETZ, which experienced salt water on all tides, tidal straining linked to an axial convergent front on the flood tide generated a lateral salinity gradient and cross-channel currents up to 0.25 m s^{-1} at the surface. This generated salinity stratification on the flood which in turn dampened turbulence, so that vertically-averaged turbulence dissipation rates were 10–50 % weaker on the flood than on the ebb, despite peak flood currents being 20–30 % stronger than ebb. Thus ebb dominance of turbulence contrasted with flood dominance of current velocity. This asymmetry reduced or disappeared on neaps when the lateral circulation was much reduced. But in the upper part of the RETZ, which received salt water only on spring tides, lateral currents did not occur as the channel was too narrow, so neither salinity stratification nor turbulence dampening occurred on the flood. Here both flood dominant velocity and turbulence prevailed. Hence there was a landward switch from ebb dominant turbulence to flood dominant turbulence within the RETZ on spring tides. These switches of turbulence asymmetry were observed on spring tides during all four periods of measurement (January, March, July, September). The turbulence asymmetry in the lower part of the RETZ diminished or disappeared on neap tides.

SPM mass concentration peaks occurred due to local resuspension and advection of an ephemeral estuarine turbidity maximum (ETM). The ETM was created by the flood tide as it advanced across intertidal sandflats in the main body of the estuary and it was carried upstream on the cusp of the saltwater intrusion. The ETM contained larger flocs than the resuspended SPM. Settling of larger flocs occurred in the RETZ at high tide slack water but the ETM was reformed and returned on the ebb as it was flushed downstream of the RETZ. Due to flocculation around high water, the ebb ETM carried larger flocs than the flood ETM.

Particulate carbon, nitrogen, phosphorus and faecal indicator organism (FIO) concentrations correlated with SPM mass concentrations

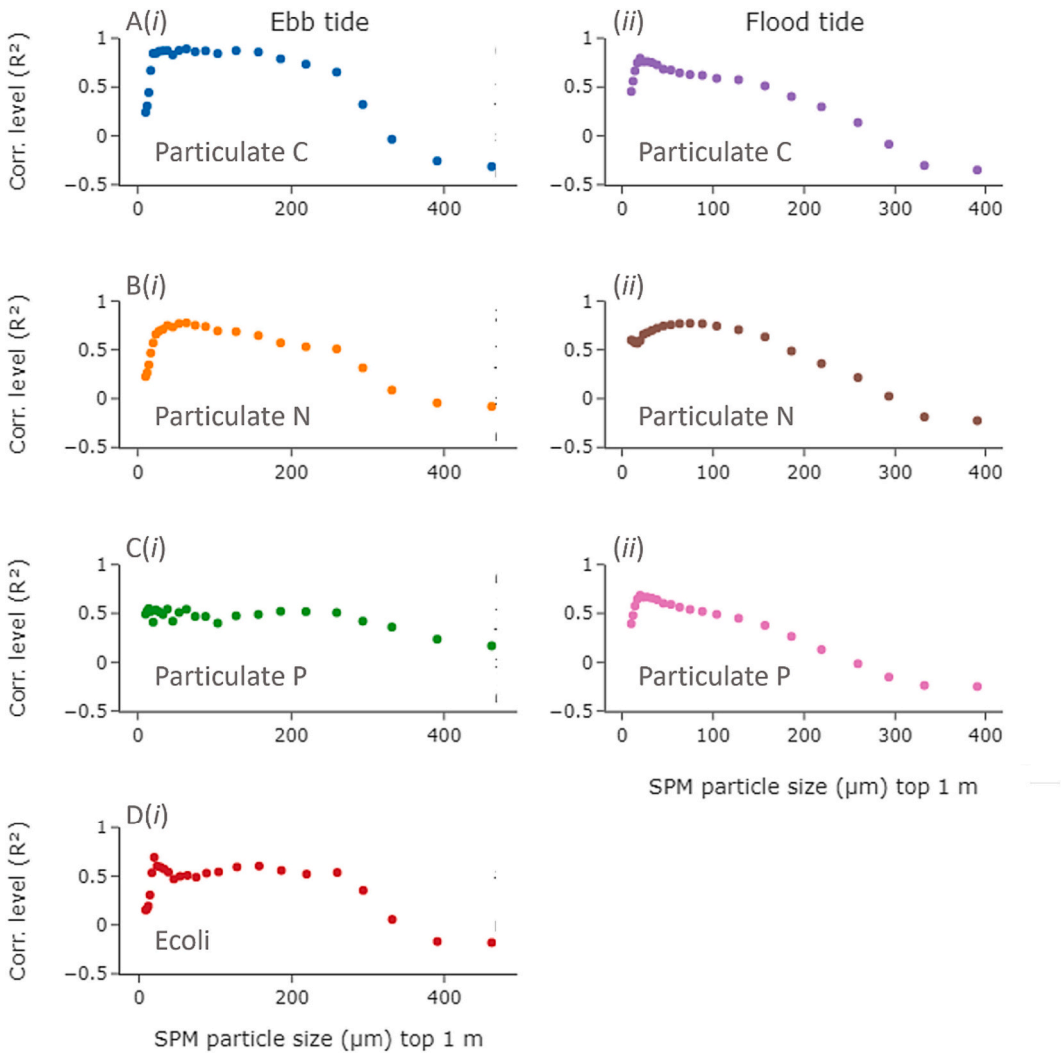

Fig. 9. Correlation values (R^2) of gross concentration of the biogeochemical component with individual particle size classes, plotted against particle size for particulate (A) carbon, (B) nitrogen, (C) phosphorus, and (D) FIOs using all samples collected during all sampling campaigns at Station 1 (Tal-y-Cafn). Left panels (i) denote correlations during the ebb tide, and right panels (ii) during the flood tide (there were not enough data for FIO analysis during the flood tide). R^2 values are statistically significant for $R^2 > 0.6$.

as maxima corresponded with resuspension and ETM advection of SPM. During periods of elevated SPM concentration, microbial water quality exceeded regulatory thresholds, emphasising the need for improved monitoring practices that consider tidal status for accurate assessment of water quality. The nutrient/FIO mass concentrations increased proportionally with the volume concentration of flocs in the 10–200 µm size range but were independent of the concentrations of very small and very large flocs. Thus it was the intermediate size flocs that were important for biogeochemical transport. There was a compositional equilibrium within the intermediate floc size range because these were mature flocs where nutrients and FIOs had transferred from dissolved to particulate phases and accumulated accordingly. By contrast, the large flocs formed in the ETM were young and had not had time to increase biogeochemical components in proportion to their increased size.

Net SPM mass fluxes over spring tides reversed direction between the upper (net landwards SPM flux) and lower (net seawards SPM flux) parts of the RETZ. Hence on spring tides the RETZ exported SPM both landwards and seawards which suggests that it was a conduit for particle bypassing rather than a sink for particle accumulation. On neap tides the net SPM flux reduced and changed direction: net flux was landward at the lower end of the RETZ and seaward at its upper end (which was then above the limit of salt penetration). Hence on neap tides the RETZ imported SPM, albeit in reduced quantities, and was a sink for particle accumulation. During a river flood event that was nearly 20 times the annual mean river discharge, the net seaward SPM flux through the lower end of the RETZ increased by two orders of magnitude.

The results of this study are likely to be applicable to many other embayment-type estuaries on macrotidal coasts, and have important implications for estuarine particulate transport, e.g., plastic dispersal, larval transport, and algal blooms, and estuary management and conservation, particularly in industries where water quality is paramount.

CRediT authorship contribution statement

Colin Jago: Writing – review & editing, Writing – original draft, Project administration, Funding acquisition, Conceptualization. **Peter Robins:** Writing – review & editing, Writing – original draft, Methodology, Investigation, Formal analysis. **Eleanor Howlett:** Writing – original draft, Visualization, Methodology, Investigation, Formal analysis, Data curation. **Francis Hassard:** Writing – review & editing, Methodology, Investigation, Formal analysis, Data curation. **Paulina Rajko-Nenow:** Investigation, Formal analysis. **Suzanna Jackson:** Investigation, Formal analysis, Data curation. **Nguyen Chien:** Writing – review & editing, Investigation, Formal analysis. **Shelagh Malham:**

Supervision, Project administration, Funding acquisition, Conceptualization.

Declaration of competing interest

The authors declare that they have no known competing financial interests or personal relationships that could have appeared to influence the work reported in this paper.

Data availability

Data will be made available on request.

Acknowledgements

This work was conducted as part of the NERC funded Macronutrients Cycles Programme: 'The Multi-Scale Response of Water quality, Biodiversity and C Sequestration to Coupled Macronutrient Cycling from Source to Sea' (Grant Number: NE/J011991/1, and see Emmett et al., 2016), which examined nutrient and pathogen fluxes through the Conwy catchment. The authors also acknowledge the NERC funded 'Microbial hitch-hikers of marine plastics: the survival, persistence & ecology of microbial communities in the Plastisphere' (Grant Number: NE/S004548/1). Field data were collected by Eleanor Howlett, Suzanna Jackson, Paulina Rajko-Nenow, Ben Powell and Gwynne Parry Jones, all at Bangor University.

Appendix A. Supplementary data

Supplementary data to this article can be found online at https://doi.org/10.1016/j.scitotenv.2024.170343.

References

Allen, G.P., Salomon, J.C., Bassoullet, P., Du Perihoat, Y., De Grandpre, C., 1980. Effects of tides on mixing and suspended sediment transport in macrotidal estuaries. Sediment. Geol. 26, 69–90.

American Public Health Association, 2018a. Standard methods committee of the American Public Health Association, American Water Works Association, and Water Environment Federation. 5310 total organic carbon (TOC). In: Baxter, T.E., Braun-Howland, E. (Eds.), Standard Methods for the Examination of Water and Wastewater. Lipps WC. APHA Press, Washington DC.

American Public Health Association, 2018b. Standard Methods Committee of the American Public Health Association, American Water Works Association, and Water Environment Federation. 4500-n nitrogen. In: Baxter, T.E., Braun-Howland, E. (Eds.), Standard Methods for the Examination of Water and Wastewater. Lipps WC. APHA Press, Washington DC.

American Public Health Association, 2018c. Standard Methods Committee of the American Public Health Association, American Water Works Association, and Water Environment Federation. 4500-p phosphorus. In: Lipps, W.C., Baxter, T.E., Braun-Howland, E. (Eds.), Standard Methods for the Examination of Water and Wastewater. APHA Press, Washington DC.

Bashawri, Y.M., Robins, P., Cooper, D.M., McDonald, J.E., Jones, D.L., Williams, A.P., 2020. Impact of sediment concentration on the survival of wastewater-derived bla CTX-M-15-producing *E. coli*, and the implications for dispersal into estuarine waters. Int. J. Environ. Res. Public Health 17 (20), 7608.

Brenon, I., Le Hir, P., 1999. Modelling the turbidity maximum in the Seine Estuary (France): identification of formation processes. Estuar. Coast. Shelf Sci. 49, 525–544.

Brown, J., Turrell, W.R., Simpson, J.H., 1991. Aerial surveys of axial convergent fronts in UK estuaries and the implications for pollution. Mar. Pollut. Bull. 22, 397–400.

Burchard, H., Schuttelaars, H.M., Ralston, D.K., 2018. Sediment trapping in estuaries. Ann. Rev. Mar. Sci. 10, 371–395.

Chernetsky, A.S., Schuttelaars, H.M., Talke, S.A., 2010. The effect of tidal asymmetry and temporal settling lag on sediment trapping in tidal estuaries. Ocean Dyn. 60, 1219–1241.

Davidson, N.C., Laffoley, D.D.A., Doody, J.P., Way, L.S., Gordon, J., Key, R.E., Drake, C. M., Pienkowski, M.W., Mitchell, R., Duff, K.L., 1991. Nature Conservation and Estuaries in Great Britain. Nature Conservancy Council, Peterborough, pp. 1–76.

Deines, K.L., 1999. Backscatter estimation using broadband acoustic Doppler current profilers. In: Proc. I.E.E.E. 6th Working Conference on Current Measurements, pp. 249–253.

Dronkers, J., 1986. Tidal asymmetry and estuarine morphology. Neth. J. Sea Res. 20, 117–131.

Droppo, I.G., 2001. Rethinking what constitutes suspended sediment. Hydrol. Process. 15, 1551–1564.

Eaton, A.D., Franson, M.A.H., 2005. Standard Methods for the Examination of Water and Wastewater. Federation. Water Environmental American Public Health Association (APHA), Washington, DC, USA, 21st edn. American Public Health Association, Washington.

Emmett, B.A., Cooper, D., Smart, S., Jackson, B., Thomas, A., Cosby, B., Evans, C., Glanville, H., McDonald, J.E., Malham, S.K., Marshall, M., 2016. Spatial patterns and environmental constraints on ecosystem services at a catchment scale. Sci. Total Environ. 572, 1586–1600.

Findlay, S., Pace, M.L., Lints, D., Cole, J.J., Caraco, N.F., Peierls, B., 1991. Weak coupling of bacterial and algal production in a heterotrophic ecosystem: the Hudson River estuary. Limnol. Oceanogr. 36, 268–278.

Golebiewski, M., Calkiewicz, J., Creer, S., Piwosz, K., 2017. Tideless estuaries in brackish seas as possible freshwater-marine transition zones for bacteria: the case study of the Vistula river estuary. Environ. Microbiol. Rep. 9 (2), 129–143. https://doi.org/10.1111/1758-2229.12509.

Ha, H.K., Mass, J.P.-Y., Park, K., Kim, Y.H., 2011. Estimation of high-resolution sediment concentration profiles in bottom boundary layer using pulse-coherent acoustic Doppler current profilers. Mar. Geol. 279, 199–209.

Hassard, F., Gwyther, C.L., Farkas, K., Andrews, A., Jones, V., Cox, B., Brett, H., Jones, D. L., McDonald, J.E., Malham, S.K., 2016. Abundance and distribution of enteric bacteria and viruses in coastal and estuarine sediments—a review. Front. Microbiol. 7, 1692.

Hassard, F., Andrews, A., Jones, D.L., Parsons, L., Jones, V., Cox, B.A., Daldorph, P., Brett, H., McDonald, J.E., Malham, S.K., 2017. Physicochemical factors influence the abundance and culturability of human enteric pathogens and fecal indicator organisms in estuarine water and sediment. Front. Microbiol. 8, 1996.

Ho, K.H., Park, K., 2012. High resolution comparison of sediment dynamics under different forcing conditions in the bottom boundary layer of a shallow, micro-tidal estuary. J. Geophys. Res. 117, C06020.

Howlett, E.R., Bowers, D.G., Malarkey, J., Jago, C.F., 2015. Stratification in the presence of an axial convergent front: causes and implications. Estuar. Coast. Shelf Sci. 161, 1–10.

Jago, C.F., 1980. Contemporary accumulation of marine sand in a macrotidal estuary, southwest Wales. Sediment. Geol. 26, 21–49.

Jago, C.F., Jones, S.E., 1998. Observation and modelling of the dynamics of benthic fluff resuspended from a sandy bed in the southern North Sea. Cont. Shelf Res. 18, 1255–1282.

Jago, C.F., Bale, A.J., Green, M.O., Howarth, M.J., Jones, S.E., McCave, I.N., Millward, G. E., Morris, A.W., Rowden, A.A., Williams, J.J., 1993. Resuspension processes and seston dynamics, southern North Sea. Philos. Trans. R. Soc. Lond. A 343, 475–491.

Jago, C.F., Jones, S.E., Sykes, P., Rippeth, T., 2006a. Temporal variation of suspended particulate matter and turbulence in a high energy, tide-stirred, coastal sea: relative contributions of resuspension and disaggregation. Cont. Shelf Res. 26, 2019–2028.

Jago, C.F., Ishak, A.K., Jones, S.E., Goff, M.R.G., 2006b. An ephemeral turbidity maximum generated by resuspension of organic-rich matter in a macrotidal estuary, S.W. Wales. Estuar. Coasts 29, 197–208.

Jago, C.F., Kennaway, G., Novarino, G., Jones, S.E., 2007. Size and settling velocity of suspended flocs during a Phaeocystis bloom in the tidally-stirred Irish Sea, N W European shelf. Mar. Ecol. Prog. Ser. 345, 51–62.

Jones, A.E., Hardison, A.K., Hodges, B.R., McClelland, J.W., Moffett, K.B., 2020. Defining a riverine tidal freshwater zone and its spatiotemporal dynamics. Water Resour. Res. 56 (4) https://doi.org/10.1029/2019WR026619 e2019WR026619.

Laprise, R., Dodson, J.J., 1994. Environmental variability as a factor controlling spatial patterns in distribution and species diversity of zooplankton in the St. Lawrence estuary. Mar. Ecol. Prog. Ser. 107, 67–81.

Levin, L.A., Boesch, D.F., Covich, A., Dahm, C., Erséus, C., Ewel, K.C., Kneib, R.T., Moldenke, A., Palmer, M.A., Snelgrove, P., Strayer, D., 2001. The function of marine critical transition zones and the importance of sediment biodiversity. Ecosystems 4, 430–451.

Malham, S.K., Rajko-Nenow, P., Howlett, E., Tuson, K.E., Perkins, T.L., Pallett, D.W., Wang, H., Jago, C.F., Jones, D.L., McDonald, J.E., 2014. The interaction of human microbial pathogens, particulate material and nutrients in estuarine environments and their impacts on recreational and shellfish waters. Environ Sci Process Impacts 16, 2145–2155.

Nunes, R., Simpson, J.H., 1985. Axial convergence in a well-mixed estuary. Estuar. Coast. Shelf Sci. 20, 637–649.

Painchaud, J., Therriault, J.C., 1989. Relationships between bacteria, phytoplankton and particulate organic carbon in the upper St. Lawrence estuary. Mar. Ecol. Prog. Ser. 56, 301–311.

Perkins, T.L., Clements, K., Baas, J.H., Jago, C.F., Jones, D.L., Malham, S.K., McDonald, J.E., 2014. Sediment composition influences spatial variation in the abundance of human pathogen indicator bacteria within an estuarine environment. PloS One 9 (11), e112951. https://doi.org/10.1371/journal.pone.0112951.

Philips, J.D., 2022. Geomorphology of the fluvial–estuarine transition zone, lower Neuse River, North Carolina. Earth Surf. Process. Landf. 47, 2044–2061. https://doi.org/10.1002/esp.5362.

Quilliam, R.S., Clements, K., Duce, C., Cottrill, S.B., Malham, S.K., Jones, D.L., 2011. Spatial variation of waterborne *Escherichia coli* — implications for routine water quality monitoring. J. Water Health 9, 734–737. https://doi.org/10.2166/wh.2011.057.

Robins, P.E., Neill, S.P., Giménez, L., 2012. A numerical study of marine larval dispersal in the presence of an axial convergent front. Estuar. Coast. Shelf Sci. 100, 172–185.

Robins, P.E., Lewis, M.J., Simpson, J.H., Howlett, E.R., Malham, S.K., 2014. Future variability of solute transport in a macrotidal estuary. Estuar. Coast. Shelf Sci. 151, 88–99.

Robins, P.E., Cooper, D., Malham, S.K., Jones, D.L., 2019. Viral dispersal in the coastal zone: a method to quantify water quality risk. Environ. Intl. 126, 430–442.
Robins, P.E., Dickson, N., Kevill, J.L., Malham, S.K., Singer, A.C., Quilliam, R.S., Jones, D.L., 2022. Predicting the dispersal of SARS-CoV-2 RNA from the wastewater treatment plant to the coast. Heliyon 8 (9), e10547.
Rusello, P.J., Cowen, E.A., 2010. Turbulent dissipation estimates from pulse coherent Doppler instruments. In: Proceedings of the IEEE/OES/CWTM Tenth Working Conference on Current Measurement Technology, pp. 167–172.
Simpson, J., Vennell, R., Souza, A.J., 2001. The salt fluxes in a tidally energetic estuary. Estuar. Coastal Shelf. Sci. 52, 131–142.
Smith, D.C., Simon, M., Alldredge, A.L., Azam, F., F., 1992. Intense hydrolytic enzyme activity on marine aggregates and implications for rapid particle dissolution. Nature 359, 139–142.
Sulaiman, Z.A., Viparelli, E., Torres, R., Yankovsky, A., Grego, J., 2021. The influence of tides on coastal plain channel geomorphology: Altamaha River, Georgia, USA. J. Geophys. Res. Earth Surf. 126 (7) https://doi.org/10.1029/2020JF005839Sun e2020JF005839.
Torres, R., 2017. Channel geomorphology and the fluvial–tidal transition, Santee River, USA. Geol. Soc. Am. Bull. 129, 1681–1692.
Turrell, W.R., Simpson, J.H., 1988. The measurement and modelling of axial convergence in shallow well-mixed estuaries. In: Dronkers, J., van Leussen, W. (Eds.), Physical Processes in Estuaries. Springer-Verlag, pp. 130–145.
Turrell, W.R., Brown, J., Simpson, J.H., 1996. Salt intrusion and secondary flow in a shallow, well-mixed estuary. Estuar. Coast. Shelf Sci. 42, 153–169.
Uncles, R.J., Jordan, M.B., 1980. A one-dimensional representation of residual currents in the Severn Estuary and associated observations. Estuar. Coast. Mar. Sci. 10, 39–60.
Uncles, R.J., Stephens, J.A., 1993. The saltwater-freshwater interface and its relationship to the turbidity maximum in the Tamar Estuary, United Kingdom. Estuaries 16, 126–141. https://doi.org/10.2307/1352770.
Uncles, R.J., Elliott, R.C.A., Weston, S.A., 1985. Dispersion of salt and suspended sediment in a partly mixed estuary. Estuaries 8, 256–269.
Vaqué, D., Pace, M.L., Findlay, S., Lints, D., 1992. Fate of bacterial production in a heterotrophic ecosystem: grazing by protists and metazoans in the Hudson estuary. Mar. Ecol. Prog. Ser. 110, 283–292.
West, J.R., Sangodoyin, A.Y.A., 1991. Depth-mean tidal current and sediment concentration relationships in three partially mixed estuaries. Estuar. Coast. Shelf Sci. 32 (2), 141–159.
West, J.R., Guymer, I., Sangodoyin, Y., Oduyemi, K.O., 1986. Solute dispersion and sediment transport in estuaries. Water Sci. Technol. 18 (4–5), 93–100.
Wiles, P.J., T.P. Rippeth, J.H. Simpson, and P.J. Hendricks. 2006. A novel technique for measuring the rate of turbulent dissipation in the marine environment. Geophys. Res. Lett. 33: p. L21608 https://doi.org/https://doi.org/10.1029/2006GL027050.
Winkler, G., Dodson, J., Bertrand, N., Thivierge, D., Vincent, W., 2003. Trophic coupling across the St. Lawrence River estuarine transition zone. Mar. Ecol. Prog. Ser. 251, 59–73.
Yu, Q., Wang, Y., Gao, S., Flemming, B., 2014. Turbidity maximum formation in a well-mixed tidal estuary: the role of tidal pumping. J. Geophys. Res. 119, 7705–7724. https://doi.org/10.1002/2014JC010228.